COMPDYN 2025
10th ECCOMAS Thematic Conference on
Computational Methods in Structural Dynamics and Earthquake Engineering
M. Papadrakakis, M. Fragiadakis (eds.)
Rhodes Island, Greece, 15-18 June 2025

METALLIC AND FLUID VISCOUS DAMPERS FOR SEISMIC PROTECTION OF INFILLED FRAME BUILDINGS

Gloria Terenzi[1], **Stefano Sorace**[2]

[1] Department of Civil and Environmental Engineering, University of Florence, Italy
Via S. Marta 3, 50139 Florence, Italy
e-mail: gloria.terenzi@unifi.it

[2] Polytechnic Department of Engineering and Architecture, University of Udine, Udine, Italy
Via delle Scienze 206, 33100 Udine, Italy
stefano.sorace@uniud.it

Abstract

Seismic retrofit of reinforced concrete (RC) frame buildings should target a proper protection not only of the structural skeleton, but also of the non-structural elements interacting with it under lateral loads, and particularly of masonry infills and partitions. Hence, the response of the latter should be properly simulated in assessment analyses carried out in current state, and the rehabilitation strategies be selected in order to provide adequate combined enhancements of structural and non-structural performance. This topic is developed in the study presented herein, where a representative case is examined, i.e. a 6-storey residential building with RC frame structure situated in L'Aquila, Italy, designed in compliance with the 1986 edition of the Italian Seismic Standards. In the assessment and retrofit design analyses, infills and partitions are modelled by means of diagonal no-tension struts with multilinear pivot-type hysteretic behaviour. Based on the response evaluated in current conditions, two different retrofit solutions are proposed, both consisting in a dissipative bracing system. In the former solution, the system is equipped with Added Damping and Stiffness (ADAS) steel devices, whereas in the latter with Pressurized Fluid Viscous (PFV) dampers.
The paper reports: the characteristics of the case study building; the computational models adopted in the analyses; the design of the two protective systems; a performance evaluation in current and retrofitted conditions; checks on the correlation of the response of the ADAS and PFV-equipped dissipative bracing systems with the hypotheses formulated in their sizing processes; and a comparison between the protection capacities offered by the two technologies.

Keywords: Seismic Retrofit, RC Structures, Infills, Dissipative Bracings, Metallic Dampers, PFV Dampers.

1 INTRODUCTION

Buildings with reinforced concrete (RC) structure designed with older Technical Standards show a significant seismic vulnerability, caused by the poor strength and ductility of RC members and the damageability of masonry infills traditionally built in contact with the frame skeleton [1-2]. This directly influences the choice and sizing of retrofit strategies, which must target an adequate combined control of earthquake-induced accelerations and displacements, in order to achieve a significant improvement both of structural and non-structural performance.

Dissipative bracing (DB) technologies can effectively meet this joint objective, provided that their design ensures a proper balance between the addition of energy dissipation and the increase in lateral stiffness that they induce. Indeed, the latter always reduces the horizontal displacements but can cause a significant increase in the base and storey shears, and thus in the stress states in the structural members and the foundations. This is particularly true for bracing systems equipped with dissipators characterized by significant damping and stiffening (DS) capacities [3], which normally respond, in mechanical terms, to a Maxwell-type rheological model (i.e. with an in-series connection of a spring and a dashpot representing the elastic and damping components of the device).

As an alternative, the incorporation of almost exclusively dissipative (AOD) devices—the behaviour of which can be schematized by a Kelvin-type rheological model (i.e. with an in-parallel spring-dashpot connection)—only slightly increases the horizontal stiffness of the structural system, since their elastic stiffness is low [3-4]. Thus, the energy dissipation capacity of AOD dissipators must be carefully calibrated at the design stage, since it represents the only source of passive seismic control in retrofitted conditions.

As common case study, a 6-storey residential block with RC structure and masonry infilled façades located in a medium-high seismicity zone in Italy is examined, representative of a wide stock of buildings with similar characteristics designed according to the 1986 edition of the National Seismic Standards [5]. The two systems are pre-sized by means of expeditious criteria recently proposed by the authors for ADAS [4,6] and PFV [7] devices. Both criteria are applied for the first time in this study by referring to the results of the seismic performance evaluation carried out in current state by including the infills in relevant finite element time-history analysis, in addition to the final verification analysis in retrofitted conditions.

The geometrical and structural characteristics of the building are presented in the second section, and the results of the analysis in current state in the third. The sizing steps of the two dissipative systems are offered in the fourth section, and a thorough performance evaluation in the two retrofitted conditions, with mutual comparisons and considerations about possible different design choices for both systems, in the fifth.

2 CASE STUDY BUILDING

As mentioned in the Introduction, the case study building was designed according to the 1986 edition of the Italian Seismic Standards [5], where a maximum ordinate of 0.07 g (g = acceleration of gravity) of the pseudo-acceleration design spectrum was set for the seismic zone that included the building site at that time. The inter-storey heights are equal to 3.4 m for the ground storey and 3.04 m for the remaining storeys. The plan is rectangular, measuring 21.05×11.45 m^2, with the long side parallel to the X axis and the short side to the Y axis of the

adopted Cartesian reference system, as shown in Figure 1, where the numbering of the column types refers to the ground storey.

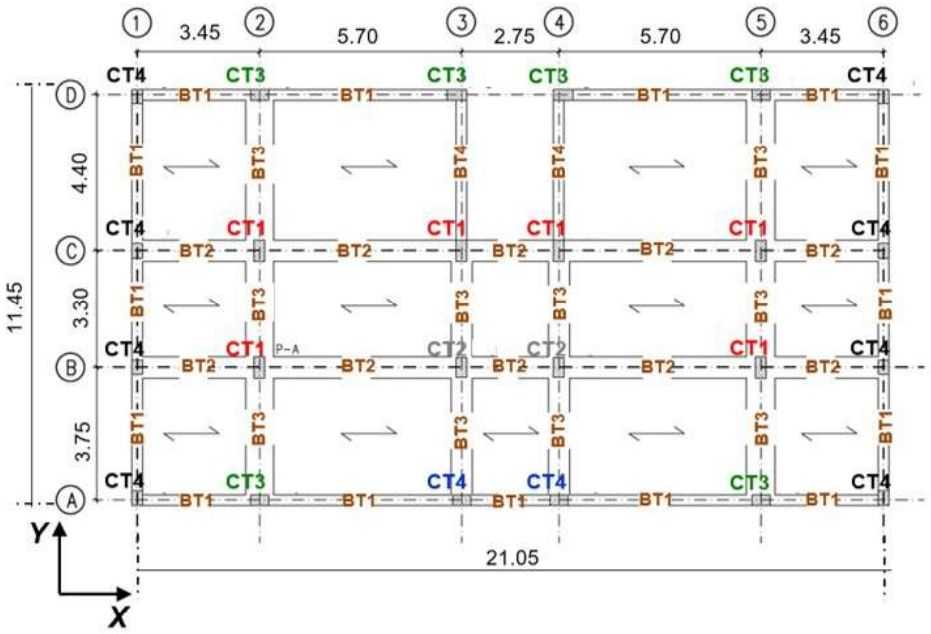

Figure 1: Structural plan of the building (dimension in meters).

Floors are made of 200 mm-high RC joists, parallel to *X*, interposed clay lug bricks, and a 50 mm-thick upper RC slab. The column cross sections are of five types, named CT1 through CT5, having the following sizes and steel reinforcing bars: CT1 – 300×600 (side parallel to *X* × side parallel to *Y*) mm^2, 8 ϕ 14; CT2 – 300×550 mm^2, 8 ϕ14; CT3 – 500×300 mm^2, 6 ϕ14; CT4 – 300×400 mm^2, 4 ϕ 14; and CT5 – 300×300 mm^2, 4 ϕ12. The transversal reinforcement is constituted by 200 mm-spaced ϕ 6 stirrups for all columns. On all storeys, perimeter beams (named BT1 in Figure 1) have out-of-depth section sized 300×500 (base × height) mm^2, with constant reinforcement given by 3 ϕ16 top bars and 2 ϕ16 bottom bars, and 200 mm-spaced ϕ 6 stirrups; internal beams parallel to *X* (BT2) have in-depth sections sized 600×250 mm^2, with a maximum of 8 ϕ16 top bars and 6 ϕ16 bottom bars, and ϕ 6 stirrups spaced from 70 mm to 200 mm; internal beams parallel to *Y* (BT3) have in-depth sections sized 800×250 mm^2, with a maximum of 8 ϕ 20 top bars and 5 ϕ 20 bottom bars, and ϕ 6 stirrups spaced from 150 mm to 200 mm.

The foundations are constituted by a mesh of inverse T-shaped RC beams. Their base sections are 2,600 mm-wide in *Y* direction and 1,600 mm-wide in *X*, with 1,200 mm (*Y*) and 800 (*X*) mm-high and 700 (*X* and *Y*) mm-wide webs, and 600 mm (*Y*) and 400 mm (*X*) mm-high flanges. Both for the elevation and foundation structures, reinforcing bars are made of FeB44k steel, with yield stress and tensile strength values greater than 430 MPa and 540 MPa, respectively; and concrete is 25/30 class, with cylindrical and cubic compressive strength of 25 MPa and 30 MPa, respectively. All infills are made of a double layer of 120 mm-thick solid bricks, and partitions of a single layer of 80 mm-thick hollow bricks, with a 65% hollow ratio over the total volume.

3 PERFORMANCE ASSESSMENT ANALYSIS IN CURRENT STATE

Views of the finite element model of the structure, generated by means of SAP2000NL software [8], are displayed in Figure 2, where the coordinate system is also plotted. As shown by the two images in Figure 2b, infills were simulated by means of pairs of equivalent crossed

compression-only resisting diagonal struts, whose cross sections were determined by using the well-established criteria formulated in [9-10]. The computed axial force-displacement response of the struts was converted into the lateral force (H_p)–drift (D_p) response of the panels using basic trigonometric relations.

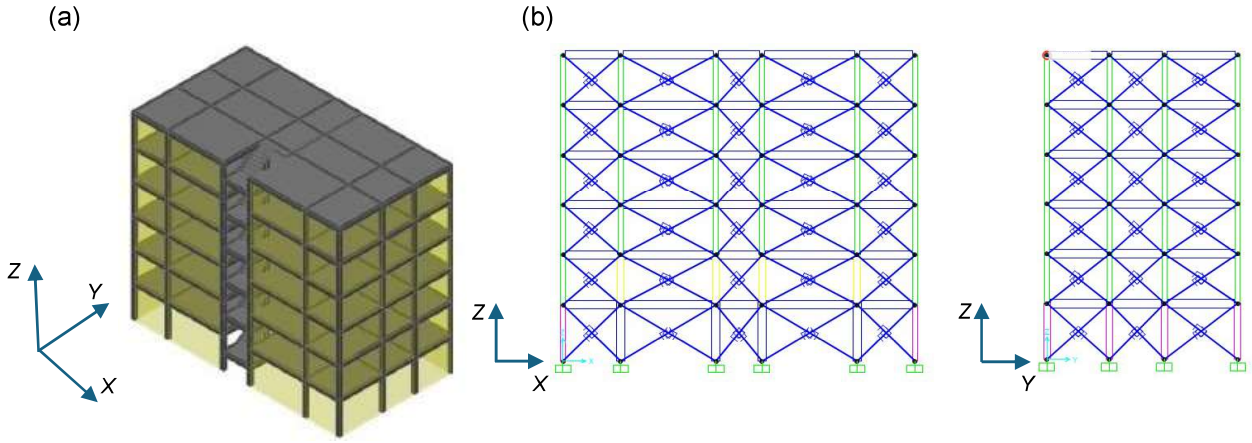

Figure 2: Views of the finite element model of the structure: (a) RC frame skeleton; (b) front and lateral views including the diagonal strut elements simulating the infills.

In continuity with a recent study by the authors' [11], the non-linear response of the panels was described by means of a trilinear backbone curve, drawn in Figure 3a in terms of normalized lateral force, H_{pr}, i.e. the ratio of H_p to the peak force of the panel, $H_{p,max}$, and normalized drift, D_{pr}, i.e. the ratio of D_p to the height of the panel, h_p. $H_{p,max}$ was computed by referring to the minimum stress value associated with the achievement of one of the four possible failure mechanisms of the panel, as defined by the classical relations presented in [10].

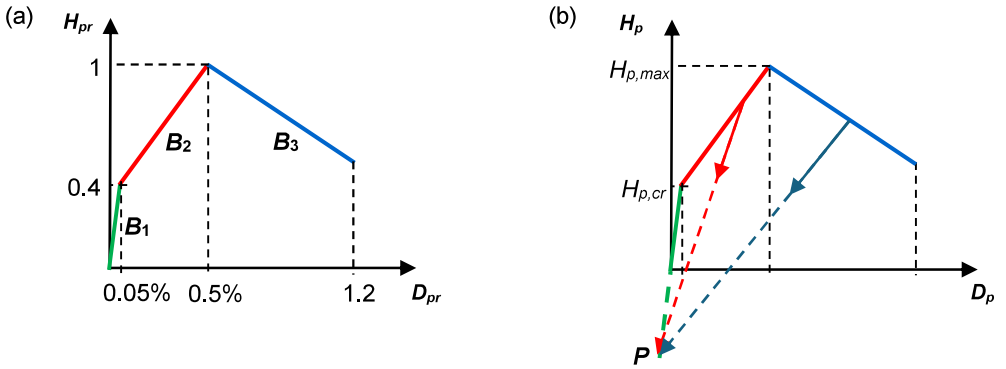

Figure 3: Normalized backbone curve (a) and pivot-type hysteretic rule (b) assumed in the analysis of infills.

The first response branch (B_1, traced out in green) corresponds to an elastic non-cracked behaviour of the panel, whose limit can be set approximately at a D_{pr} value of 0.05% [11] and a normalized cracking lateral force of the panel, $H_{pr,cr}$ (ratio of the cracking lateral force, $H_{p,cr}$, to $H_{p,max}$) equal to about 0.4 [11,12-13]. The second branch (B_2, yellow) is characterized by an increasing number of cracks in the panels and detachments from the adjacent columns and the upper beams. The drift ratio limit of this branch, coinciding with the attainment of the peak normalized force (H_{pr} = 1), is set at 0.5%, i.e. the value established by most Seismic Standards as the threshold of the Immediate Occupancy performance level (hereafter referred to as $D_{pr,IO}$). The third branch (B_3, blue) is characterized by a negative slope, measured by an angle

equal or slightly greater than 30° [11,13], and defines a progressively increasing damage, still repairable below 0.8% [13]. The end of this branch is fixed at a value of 1.2% (named $D_{pr,u}$ in the following), where collapse conditions for solid brick panels can be technically assumed. Given the small thickness and high hollow ratio of the constituting blocks, the partitions were not included in the finite element analyses.

The hysteretic behaviour of the infill panels was reproduced by a multilinear no-tension pivot-type rule included in the SAP2000NL library. This rule is plotted in the unnormalized $H_p - D_p$ response graph in Figure 3b, where the pivot point is indicated by the letter P. A modal analysis was initially carried out on the infilled structure, which showed two main translational modes, with vibration periods equal to 0.864 s along X ($T_{C,X}$) and 0.811 s ($T_{C,Y}$) along Y, and effective modal masses of 88.3% (X) and 87.9% (Y) of the total seismic mass M of the building, equal to $1.675 \cdot 10^4$ kN/g. Period and effective mass of the first rotational mode around the vertical axis Z are equal to 0.233 s and 56.5%, respectively. The seismic assessment study of the infilled structure was developed via time-history analysis by using as input a set of seven groups of three accelerograms. For each group, one accelerogram was applied in X direction, one in Y, and one in Z. The artificial ground motions were generated from the elastic pseudo-acceleration response spectra with linear viscous damping ratio equal to 0.05 (Figure 4) assumed by the current Italian Technical Standards [14], which classify the building site as a medium-high seismicity zone.

The three spectral graphs for the two horizontal components and the three graphs for the vertical one are referred to the Serviceability Design Earthquake (SDE, characterized by 63% probability of being exceeded over the reference structural lifespan, V_R), Basic Design Earthquake (BDE, with 10%/V_R probability) and Maximum Considered Earthquake (MCE, with 5%/V_R probability) hazard levels, for C-type (i.e. medium-dense sand) soil and T1-type (i.e. flat surface) topographic category.

The results of the analysis in current state are synthesized in Figures 4 through 6. Figure 4 shows the maximum infill drift ratio, $D_{pr,max}$, profiles, along X and Y directions, for the three hazard levels. The highest drifts are reached on the second storey for both axes and for all hazard levels. At the SDE, $D_{pr,max}$ values exceeding the $D_{pr,IO}$ limit (identified by a dashed line in Figure 4, along with $D_{pr,u}$) are found on the second and third storey in X, and exactly reaching $D_{pr,IO}$ on the second storey in Y. At the BDE, the $D_{pr,u}$ limit is exceeded on the second and third storey, in X; the $D_{pr,max}$ values are anyway greater than 1% on the ground and first storey, and the $D_{pr,IO}$ on the fourth. At the MCE, $D_{pr,u}$ is also exceeded on the third storey, with irreparable damage conditions on the ground (in X and Y) and fourth storey (in X), and severe damage on the latter in Y. It can be noted that, due to the substantial regularity of the building in plan and elevation, differences no greater than 3.5% are found among the maximum drifts of all panels at each storey, both in X and Y. Hence, the observations drawn from the drift profiles in Figure 4 can be extended, with very little scattering, to all the infills of the building. By way of example of these results, the H_{pr}-D_{pr} response cycles of the panels embedded in the vertical alignments between the fixed lines 2/A and 3/A, parallel to X, and the fixed lines 6/C and 6/D, parallel to Y, are plotted in Figures 5 and 6, for the most demanding BDE-scaled group of accelerograms.

The checks carried out on the structural members in terms of stress states highlight 22%, 72%, and 81% of columns, and 18%, 68%, and 76% of beams in unsafe conditions at the SDE, BDE, and MCE, respectively. The maximum demand/capacity ratios of columns in compression/flexure at the BDE result as follows, on the six storeys: 2.47—ground; 2.68—first; 2.61—second; 2.34—third; 2.39—fourth; 2.15—fifth. The maximum demand/capacity ratios of beams in flexure are equal to: 2.03—ground; 2.27—first; 2.22—second; 2.01—third;

2.03—fourth; 1.86—fifth. The maximum ratios in shear are averagely 10% lower than in flexure.

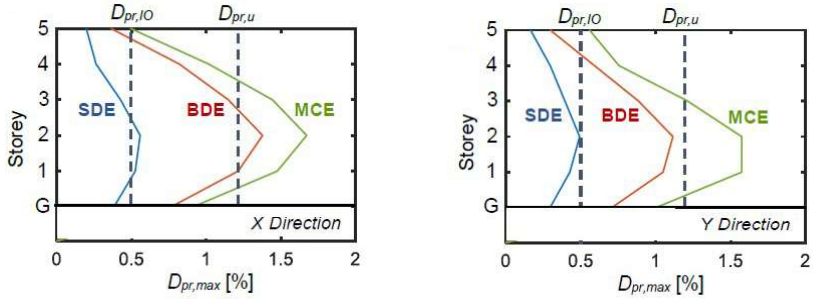

Figure 4: Maximum infill drift ratio profiles obtained for the SDE, BDE and MCE-scaled seismic action in *X* and *Y*.

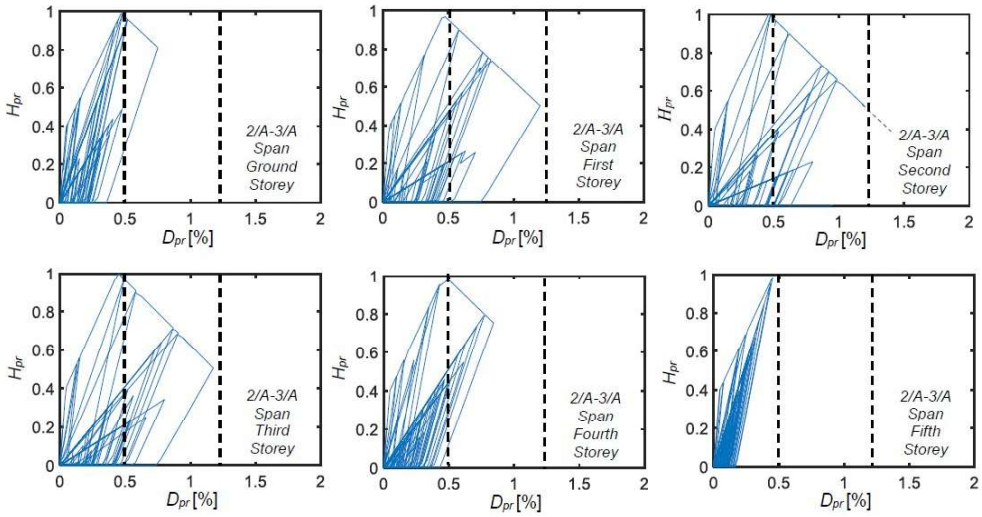

Figure 5: H_{pr}-D_{pr} response cycles of the infill panels situated in the 2/A-3/A spans obtained from the most demanding BDE-scaled group of accelerograms.

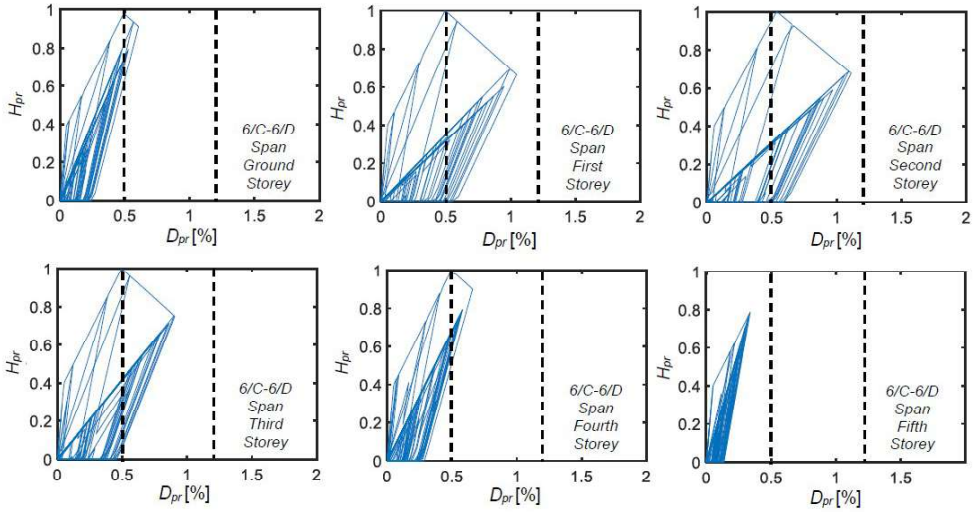

Figure 6: H_{pr}-D_{pr} response cycles of the infill panels situated in the 6/C-6/D spans obtained from the most demanding BDE-scaled group of accelerograms.

4 RETROFIT INTERVENTION WITH ADAS DAMPERS

The geometry and the idealized bilinear strain hardening force (F_p)–displacement (d_p) hysteretic cycle of a plate constituting the ADAS devices adopted here, characterized by a triangular shape, are shown in Figure 7. The following symbols are used in these drawings to describe the plate geometry and cyclic response: B_p, A_p, t_p = base, height and thickness; $F_{p,max+}$, $F_{p,max-}$, $d_{p,max+}$, $d_{p,max-}$ = maximum positive and negative force and displacement; $E_{D,p,cap}$ = energy dissipated by the plate in the maximum response cycle, delimited by the points ($F_{p,max+}$, $d_{p,max+}$), ($F_{p,max-}$, $d_{p,max-}$).

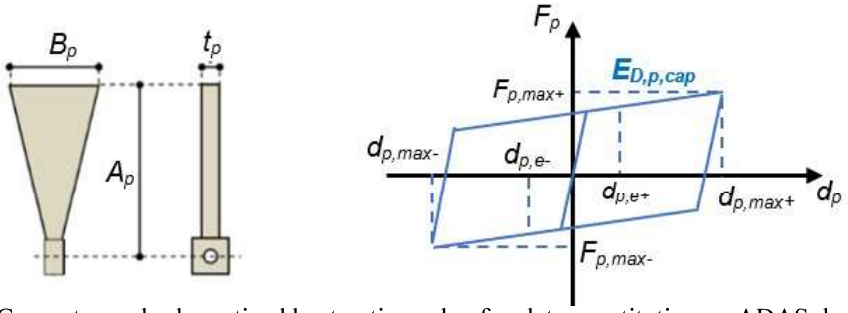

Figure 7: Geometry and schematized hysteretic cycle of a plate constituting an ADAS damper.

The preliminary design procedure of the dampers, recently formulated by the first author [4], is aimed at estimating the energy dissipation capacity of the protective system, $E_{D,S}$, by which a pre-established reduction of lateral displacements and base shear is attained. The tentative estimate of $E_{D,S}$, named $E_{D,S,t}$, is expressed as follows:

$$E_{D,S,t} = 4\Delta S_{D-}\Delta S_{A-,diss}M \tag{1}$$

where: ΔS_{D-} is the reduction of the spectral displacement, S_D, calculated for the fundamental period of the structure in current state, T_C, needed to bring $S_D(T_C)$ to a target design value in retrofitted conditions, $S_{D,t}$ ($S_{D,t} = S_D(T_C) - \Delta S_{D-}$); $\Delta S_{A-,diss}$ is the reduction of the spectral acceleration, S_A, produced by the damping action of the DB system; and M the afore-mentioned seismic mass of the building. By calculating $E_{D,S,t}$ for the two axes in plan, $E_{D,S,t,X}$, $E_{D,S,t,Y}$, the corresponding total numbers of plates to be installed in the system, N_{pX}, N_{pY}, are obtained by dividing $E_{D,S,t,X}$, $E_{D,S,t,Y}$ by the estimated value of the total energy dissipated by a plate under the input ground motions assumed in the design analyses, $E_{D,p,tot}$:

$$N_{pX(Y)} = \frac{E_{D,S,t,X(Y)}}{E_{D,p,tot}} \tag{2}$$

$E_{D,p,tot}$ is obtained by initially computing the energy dissipated by a plate in a cycle bounded by the maximum estimated positive or negative displacement, $d_{p,e}$ (also symbolically indicated, with both signs, in the graph of Figure 7), $E_{D,p,m}$; then, the contribution of the energy dissipated in all remaining cycles must be added, which is synthetically expressed by the product of $E_{D,p,m}$ and an equivalent cycle-counting factor, n_c, bringing to the following $E_{D,p,tot}$ estimate [4]:

$$E_{D,p,tot} = (1 + n_c)E_{D,p,m} \tag{3}$$

A value of 10 can be tentatively assigned to n_c for structures with fundamental periods lower than about 1.5 s [4, 15-16]. For the application of (2), (3), $E_{D,p,m}$ must be calculated, and thus $d_{p,e}$ needs to be preliminarily quantified. By considering that the supporting diagonal braces of the ADAS devices are remarkably stiff at the horizontal translation, and therefore the lateral displacements are mainly determined by the plastic deformation of the dissipators

[15], $d_{p,e}$ can be approximately assumed to coincide, storey by storey, with the maximum inter-storey drift, $D_{i,max}$ [15-16]. Then, the $E_{D,p,m}$ and $E_{D,p,tot}$ estimates are obtained by assuming a target design value for $D_{i,max}$, $D_{i,max,t}$, based on the performance capacities requested in the retrofit design. The numbers of plates to be installed on the various storeys are fixed in rounded proportion to the inter-storey drift profiles in current conditions. Therefore, the following tentative design values are assumed per each vertical alignment: 8 plates in X and 6 plates in Y on the ground storey; 10 (X) and 8 (Y) on the first; 10 (X) and 8 (Y) on the second; 8 (X) and 6 (Y) on the third; 6 (X) and 4 (Y) on the fourth, for a total of 42 plates in X and 32 plates in Y. Multiplying these number by the 8 alignments per axis, the resulting total design numbers of plates in X, $N_{p,d,X}$, and Y, $N_{p,d,Y}$, are: $N_{p,d,X}$ = 336, $N_{p,d,Y}$ = 256. The two values are about 10% greater than the corresponding values estimated by the sizing criterion, $N_{p,X}$ = 306 and $N_{p,Y}$ = 233. This allows to preserve a margin of energy dissipation capacity with respect to the MCE-scaled input action. No plates are installed on the upper storey, due to the elastic response of its structural members and the small drifts computed in current state. However, traditional non-dissipative braces are mounted on this storey, so as to prevent discontinuities in the lateral stiffness of the structure along the height of the building. A circular tubular section with 150 mm diameter and 4.6 mm thickness is adopted for the steel braces on all storeys.

5 RETROFIT INTERVENTION WITH PFV DAMPERS

The mechanical behaviour of the considered class of pressurized fluid viscous devices, whose working principle is based on the flow of a highly viscous fluid through a thin annular space between the piston head and the tank casing, is characterized by a total reaction force, F_t, given by the sum of the following damping, F_D, and elastic, F_{ne}, components [18]:

$$F_D(t) = csgn\left[\dot{d}(t)\right]\left|\dot{d}(t)\right|^{\gamma} \tag{4}$$

$$F_{ne}(t) = k_2 d(t) + \frac{(k_1 - k_2)d(t)}{\left[1+\left|\frac{k_1 d(t)}{F_0}\right|^5\right]^{1/5}} \tag{5}$$

where: t = time variable; c = damping coefficient; $sgn(\cdot)$ = signum function; $\dot{d}(t)$ = velocity; $|\cdot|$ = absolute value: γ = fractional exponent, ranging from 0.1 to 0.2; F_0 = static pre-load; k_1, k_2 = stiffness of the response branches situated below and beyond F_0; and $d(t)$ = displacement. The PFV devices are installed in pairs in dissipative bracing systems [4], with pistons driven in half-stroke position at the tip of the supporting V-shaped steel trusses, to obtain a symmetric tension-compression response capacity. A schematic hysteretic cycle of a spring-damper is traced out in Figure 8, where $F_{D,max}$, $F_{ne,max}$ are the maximum response values of F_D and F_{ne}, $F_{t,max}$ is the corresponding maximum F_t value, given by the sum of F_{Dmax} and $F_{ne,max}$, d_{max} is the piston stroke and $\pm d_{max}/2$ is the half-stroke mounting position.

The preliminary sizing procedure of PFV dissipators applied herein is based on a quick estimation of the energy dissipation capacity of the protective system by which a pre-established reduction of storey shears is attained [7]. The procedure starts from the computation of the α_V ratio between the maximum storey shear demand in current state, $V_{std,C}$, and the storey shear strength, $V_{sts,C}$, given by the sum of the elastic shear strength of the structure and the $H_{p,max}$ peak forces of all infills:

$$\alpha_V = \frac{V_{std,C}}{V_{sts,C}} \tag{6}$$

Based on α_V, the total energy dissipation demanded to the set of PFV dampers to be installed on a storey, $E_{D,\alpha V,t}$ is estimated by the following relation [7]:

$$E_{D,\alpha V,t} = 4(\alpha_V - 1)V_{sts,C}D_{i,max,t} \quad (7)$$

where $D_{i,max,t}$ is the tentatively assumed target inter-storey drift, as defined in the pre-sizing process of ADAS dampers.

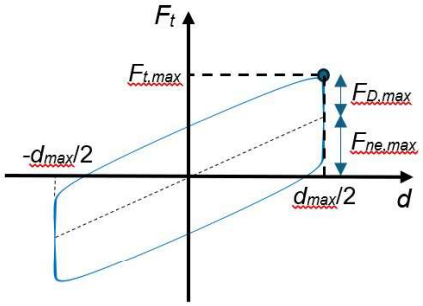

Figure 8: Schematic hysteretic cycle of a PFV spring-damper in half-stroke mounting configuration.

By calculating the energy dissipation capacity corresponding to the targeted maximum $D_{i,max,t}$ drifts, $E_{cap}(D_{i,max,t})$, the following values are obtained:
A: $E_{cap}(D_{i,max,t}) = E_{cap}(\pm 12.2 \text{ mm}) = E_{cap,max} \cdot (12.2/20) = 1.22$ kJ;
B: $E_{cap}(D_{i,max,t}) = E_{cap}(\pm 15.2 \text{ mm}) = E_{cap,max} \cdot (15.2/25) = 3.33$ kJ;
C: $E_{cap}(D_{i,max,t}) = E_{cap}(\pm 15.2 \text{ mm}) = E_{cap,max} \cdot (15.2/30) = 5.88$ kJ.

By referring to these $E_{cap}(D_{i,max,t})$ values, the devices recapitulated below are selected to obtain total energy dissipation capacities for the set of dissipators to be installed on each storey, $E_{cap,tot}(D_{i,max,t})$, greater than the corresponding $E_{D,\alpha V,mc,t}$ values listed above, in X and Y.

Ground, first and second storey: X – 4 C_{PFV}, in 3/A-4/A, 3/B-4/B spans, and 8 B_{PFV}, in 1/A-2/A, 5/A-6/A, 1/D-2/D, 5/D-6/D spans ($E_{cap,tot,X}(D_{i,max,t})$ = 50.2 kJ); Y – 16 B_{PFV} ($E_{cap,tot,Y}(D_{i,max,t})$ = 53.3 kJ);

Third storey: X – 4 B_{PFV}, in 3/A-4/A, 3/B-4/B spans, and 8 A_{PFV}, in 1/A-2/A, 5/A-6/A, 1/D-2/D, 5/D-6/D spans ($E_{cap,tot,X}(D_{i,max,t})$ = 29.8 kJ); Y – 8 B_{PFV}, in 1/A-1/B, 1/C-1/D, 6/A-6/B, 6/C-6/D spans, and 8 A_{PFV}, in 2/A-2/B, 2/C-2/D, 5/A-5/B, 5/C-5/D spans ($E_{cap,tot,Y}(D_{i,max,t})$ = 36.4 kJ);

Fourth storey: 12 A_{PFV} ($E_{cap,tot,X}(D_{i,max,t})$ = 14.6 kJ); Y – 16 A_{PFV} ($E_{cap,tot,Y}(D_{i,max,t})$ = 19.5 kJ).

Like for the ADAS-based retrofit solution, no dampers are installed in the braces of the fifth storey. A 4.6 mm-thick circular tubular section with a diameter of 139 mm is selected for the braces on all storeys.

6 PERFORMANCE ASSESSMENT ANALYSIS IN RETROFITTED CONDITIONS

6.1 ADAS-based retrofit solution

Like in current state, the modal analysis in ADAS-based retrofitted conditions shows two main translational modes, with periods of 0.476 s in X ($T_{ADAS,X}$) and 0.463 s in Y ($T_{ADAS,Y}$), and effective modal masses equal to 83.8% and 84.6% of M. The periods are 5.1% and 6.2% greater than the corresponding $T_{R,X}$ = 0,453 s and $T_{R,Y}$ = 0.436 s values computed at the pre-sizing stage, respectively. At the same time, $T_{ADAS,X}$, $T_{ADAS,Y}$ are equal to 55.1% and 57.1% of the $T_{C,X}$ = 0.864 s and $T_{C,Y}$ = 0.811 s period values in current state, as a consequence of the stiffening effects typically produced by the ADAS technology. This is also reflected on the first rotational mode period in retrofitted conditions, equal to 0.172 s, with effective modal mass equal to 54.3% of M, as compared to the 0.293 s value in current state. Like in current state too, a total of nine modes is needed to activate summed modal masses greater than 90%

along X and Y, and around Z. The results of the time-history analyses are synthesized in Figures 9-11, which duplicate Figures 4-6 shown above in current state.

By comparing the profiles in Figure 9 to the corresponding ones in Figure 5, the following maximum reduction factors on the peak panel drift ratios, $r_{pdr,max}$, are found in passing from current to retrofitted conditions for the three seismic hazard levels, all reached on the first storey: $r_{pdr,max}$ = 2.57 (SDE), 2.29 (BDE), 2.23 (MCE) in X, $r_{pdr,max}$ = 1.92 (SDE), 1.73 (BDE), 1.7 (MCE) in Y. The average values of the reduction factors calculated over the six storeys, $r_{pdr,ave}$, are: $r_{pdr,ave}$ = 2.43 (SDE), 2.03 (BDE), 1.98 (MCE) in X, $r_{pdr,ave}$ = 1.87 (SDE), 1.68 (BDE), 1.67 (MCE) in Y. The $r_{pdr,max}$ and $r_{pdr,ave}$ values computed in X are about 25% through 30% greater than the values in Y, as a consequence of the proportionally higher displacement and panel drift demands highlighted in current state along the first axis. This allows attaining a similar response in retrofitted conditions along the two directions at the SDE and the BDE, as also visualized, for the latter, by the H_{pr}-D_{pr} response cycles of the panels located in the spans 2/A-3/A, parallel to X (Figure 10), and 6/C-6/D, parallel to Y (Figure 11).

The peak drift ratios of both panels are limited below 0.65% on the first and second storey, corresponding to easily repairable damage conditions. At the same time, they are below the IO-related 0.5% limit on the ground, third and fourth storey. At the MCE the maximum drift ratios are well below the 0.8% technical threshold of repairability for all storeys except for the first, where this limit is only slightly exceeded ($D_{pr,max}$ = 0.81%) by two panels located in the Y-parallel alignments.

The demand/capacity ratios of columns reach maximum values of 1.25, 1.05 and 1.02 on the ground, first and second storey, respectively, whereas they are below 1 on the remaining storeys. The increase in axial force induced by the bracing effect of the protection system is safely absorbed by all columns, but not by the foundation beams parallel to X, as commented below. The beams in unsafe conditions are those connecting columns B/2 to C/2, A/3 to B/3 and C/3, A/4 to B/4, C/4 to B/5 and C/5, with maximum demand/capacity ratios ranging from 1.09 to 1.18 for bending moment, and from 1.02 to 1.13 for shear. Given the low unsafe levels evaluated for all members mentioned above, limited supplementary strengthening interventions consisting in bonding single sheets of carbon fiber reinforced (CFR) fabrics are sufficient on all of them, according to a combined ADAS-CFR retrofit strategy lately applied to RC structures [19].

At the BDE, the energy dissipated by the plates in their maximum response cycles is as follows: 0.32 kNm – ground storey, 0.33 kNm – first, 0.27 kNm – second, 0.22 kNm – third, 0.2 kNm – fourth, in X; 0.31 kNm – ground, 0.29 kNm – first, 0.25 kNm – second, 0.11 kNm – third, 0.09 kNm – fourth, in Y. The values computed for the ground and first storey in both directions are close to the pre-sizing estimate $E_{D,p,m}$ = 0.31 kNm, as a consequence of the fact that the tentatively predicted maximum displacement $d_{p,e}$ of 17 mm is nearly reached by the plates installed on these storeys. The values of the total energy dissipated in all response cycles by these plates, equal to: 3.33 kNm – ground, 3.45 kNm – first, in 1/A-2/A span; 3.28 kNmm – ground, 3.19 kNmm – first, in 1/C-1/D span, are in turn similar to the $E_{D,p,tot}$ estimate of 3.41 kNm calculated by means of relation (3). The resulting ratio of the total dissipated energy to the energy dissipated in the largest cycle approximately ranges from 10 to 12 for these plates. This holds true also for the plates mounted on the remaining storeys, confirming that the value of 10 assigned to n_c, which results in a value of 11 for the dissipated energy ratio, represents an acceptable assumption for structures— such as the case study one—with fundamental periods lower than 1.5 s.

The stress state checks on the foundation beams and the underlying soil, which were examined separately to limit the size of the finite element model of the structure in the time-history analyses, are passed by the beams parallel to Y.

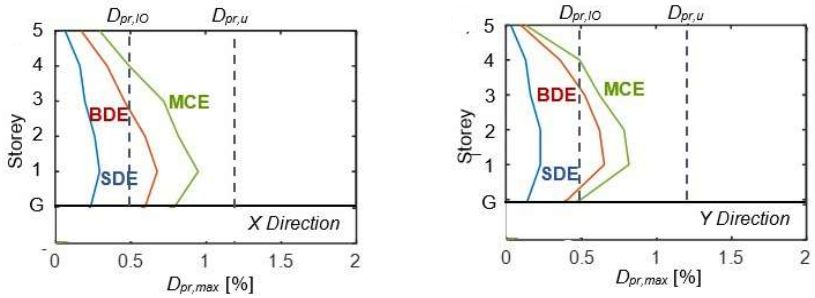

Figure 9: Maximum infill drift ratio profiles obtained for the SDE, BDE and MCE-scaled seismic action in *X* and *Y*, for the ADAS-based retrofit solution.

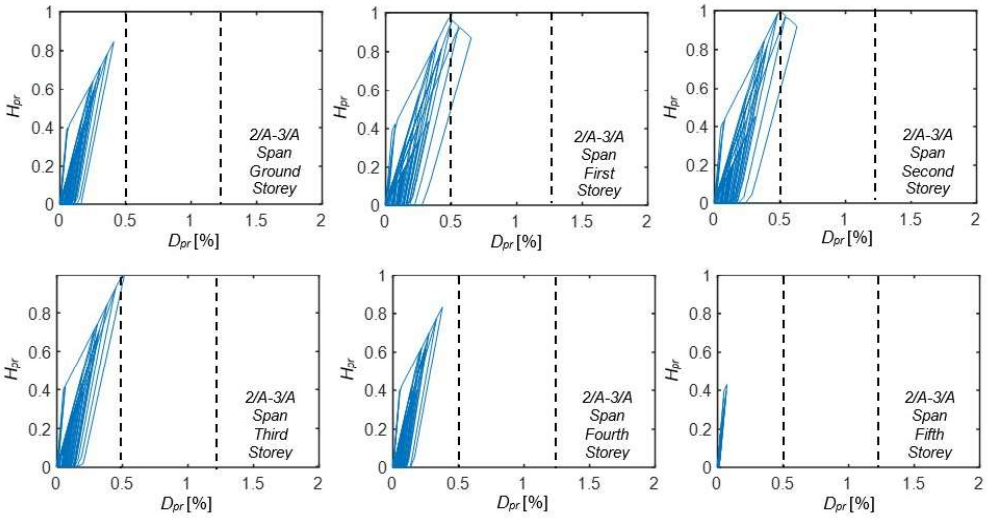

Figure 10: H_{pr}-D_{pr} response cycles of the infill panels situated in the 2/A-3/A spans obtained from the most demanding BDE-scaled groups of accelerograms, for the ADAS-based retrofit solution.

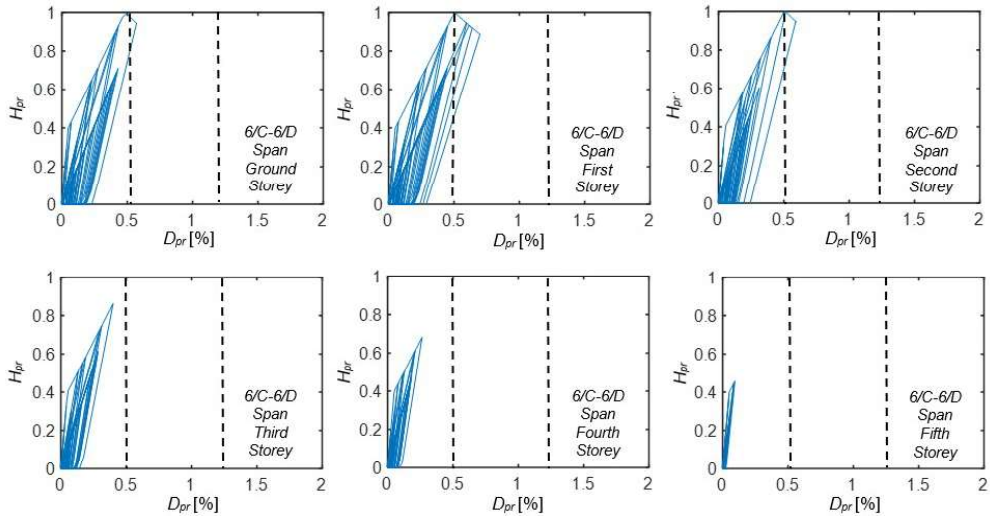

Figure 11: H_{pr}-D_{pr} response cycles of the infill panels situated in the 6/C-6/D spans obtained from the most demanding BDE-scaled groups of accelerograms, for the ADAS-based retrofit solution.

The *X*-aligned beams benefit from the significant reduction in bending moments on the base sections of the ground storey columns, and thus their section height and reinforcement do not need to be increased. At the same time, their flanges need to be widened from 1,600 mm to 2,200 mm to meet the checks on the soil, due to the above-mentioned growth of the

axial force in the ground storey columns produced by the bracing effect of the protection system, which ranges from about 20% to 30%, as compared to current conditions, for the various columns.

The post-intervention energy response time-histories at the BDE, plotted in Figure 12, highlight a contribution of the dissipative bracing system, $E_{D,ADAS}$, to the total input energy, E_I, equal to 63.2%, with 12.1% and 24.7% due to the energy produced by the slight residual hysteretic response of infills, $E_{D,INF}$, and by the modal damping, E_M, respectively.

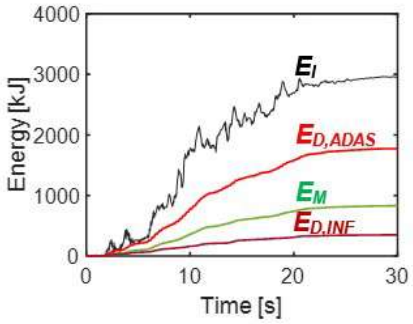

Figure 12: Energy time histories obtained from the most demanding BDE-scaled groups of accelerograms for the ADAS-based retrofit solution.

6.2 PFV-based retrofit solution

The modal analysis highlights two main translational modes also in PFV-based retrofitted conditions, with periods of 0.813 s along X ($T_{PFV,X}$), equal to 94.1% of $T_{C,X}$, and 0.767 s along Y ($T_{PFV,Y}$), i.e. equal to 94.6% of $T_{C,Y}$, as a consequence of the small stiffening effects induced by this AOD retrofit strategy. The effective modal masses are equal to 84.2% and 82.9% of M, respectively. Period and effective mass of the first rotational mode are equal to 0.251 s and 53.2%. Like for the current state and the ADAS-based retrofit, nine modes are needed to activate summed modal masses greater than 90% along X, Y, and around Z. The results of the time-history analyses are summarized in Figures 13-15, which replicate Figures 4-6 in current state and Figs. 9-11 in ADAS-retrofitted configuration.

The $r_{pdr,max}$ maximum reduction factors on the peak panel drift ratios, attained on the first storey in this case too, are as follows: $r_{pdr,max}$ = 2.68 (SDE), 2.49 (BDE), 2.43 (MCE) in X, $r_{pdr,max}$ = 2.98 (SDE), 2.65 (BDE), 2.76 (MCE) in Y. The $r_{pdr,ave}$ average values of the reduction factors on the set of six storeys are: $r_{pdr,ave}$ = 2.57 (SDE), 2.46 (BDE), 2.36 (MCE) in X, $r_{pdr,ave}$ = 2.81 (SDE), 2.51 (BDE), 2.62 (MCE) in Y. As also highlighted by Figure 13, the reduction factors are greater than the corresponding ones in the ADAS-based retrofit, especially in Y, and more homogeneous along the building height. As a consequence, smoother infill drift profiles result.

The H_{pr}-D_{pr} response cycles of the panels situated in 2/A-3/A span (Figure 14), which are the most stressed along X also for this retrofit solution, slightly exceed the 0.5% drift ratio limit related to the IO performance level on the second and third storey at the BDE, reaching a maximum of 0.54%. The infills located in the 6/C-6/D span (Figure 15), most stressed in Y, show peak drifts not exceeding 0.42%, similar to the other Y-parallel panels. The maximum drifts at the MCE are no greater than 0.65% for all infills in both directions. All columns and all beams result to be in safe conditions.

The energy dissipated by the PFV damper pairs in the maximum response cycle, $E_{D,c,max}$, and in total, $E_{D,tot}$, are as follows: $E_{D,c,max}$ = 6.86 kJ (about 3.43 kJ per device), $E_{D,tot}$ = 71.66 kJ (35.83 kJ per device), C-type; $E_{D,c,max}$ = 2.94 kJ (1.47 kJ per device), $E_{D,tot}$ = 35.03 kJ (17.51 kJ per device), B-type; $E_{D,c,max}$ = 0.82 kJ (0.41 kJ per device), $E_{D,tot}$ = 9.94 kJ (4.97 kJ per device), A-type.

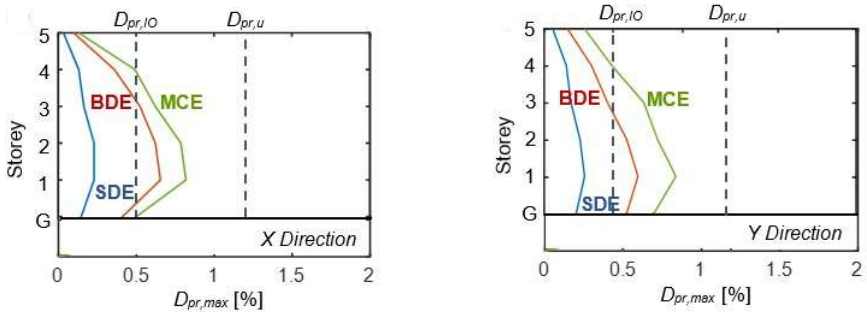

Figure 13: Maximum infill drift ratio profiles obtained for the SDE, BDE and MCE-scaled seismic action in *X* and *Y*, for the PFV-based retrofit solution.

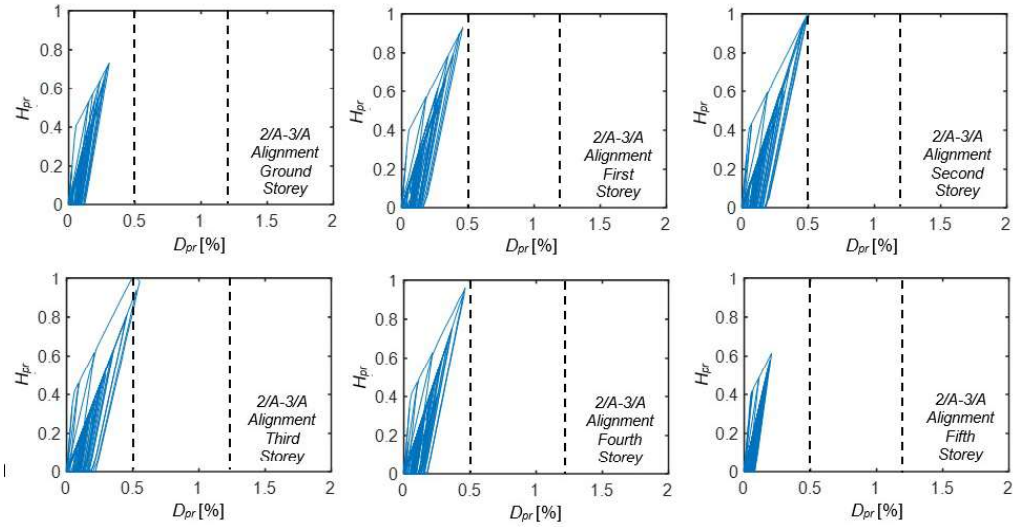

Figure 14: H_{pr}-D_{pr} response cycles of the infill panels situated in the 2/A-3/A spans obtained from the most demanding BDE-scaled groups of accelerograms, for the PFV-based retrofit solution

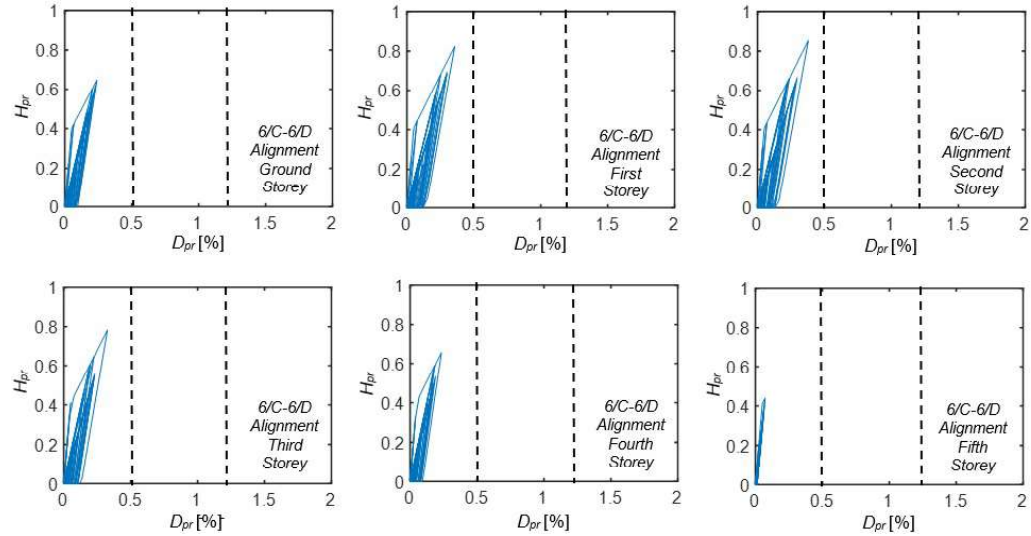

Figure 15: H_{pr}-D_{pr} response cycles of the infill panels situated in the 6/C-6/D spans obtained from the most demanding BDE-scaled groups of accelerograms, for the PFV-based retrofit solution.

These energy values are in the same proportion to the $E_{cap}(D_{i,max,t})$ values as are the maximum displacements obtained from the analysis to the $D_{i,max,t}$ tentative displacements assumed

in the sizing process. The energy response time-histories at the BDE, graphed in Figure 16, show a nearly equal final value of the input energy as compared to the value computed for the ADAS-based retrofit solution (E_I = 2953 kJ—PFV, against E_I = 2986 kJ—ADAS). The contribution of the dissipative bracing system, $E_{D,PFV}$, in this case is equal to 77.9% of E_I, with 3.1% and 19% contributions associated with the $E_{D,INF}$ minimal residual hysteretic response of infills and the E_M modal damping, respectively. The maximum displacements of the dissipators computed for the action scaled at the MCE are about 20% greater than for the BDE, resulting in peak values of 16.1 mm (C-type), 15.6 mm (B) and 10.8 mm (A). These values are significantly smaller than the strokes of ±40 mm (C), ±30 mm (B) and ±20 mm (A). Thanks to the low stiffening effects of the dissipative bracing system incorporating the PFV devices, the corresponding small increase in the axial force of the columns does not require flange-widening interventions on the foundation beams.

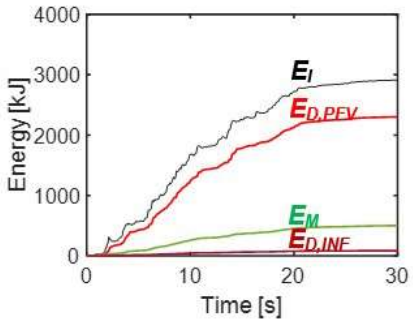

Figure 16: Energy time histories obtained from the most demanding BDE-scaled groups of accelerograms for the PFV-based retrofit solution.

5 CONCLUSIONS

The design of the ADAS-based and PFV-based dissipative bracing solutions for the building examined in this article provided the opportunity for an uncommon direct comparison of their performance for the same seismic retrofit case study. Both systems were pre-sized for the first time basing relevant procedures—recently formulated by the authors—on the results of the performance evaluation in current state carried out including the infills in the finite element time-history analyses.

Detailed remarks derived from the results of the study are summarized below.

– In current conditions, the second and third storey infills of the building exceed the $D_{pr,IO}$ limit at the SDE, and the $D_{pr,u}$ limit at the BDE; moreover, panel drifts notably higher than $D_{pr,IO}$ are always found at the BDE, assessing irreparable damage (ground and first storey) or severe damage (fourth). At the MCE, $D_{pr,u}$ is also exceeded on the third storey, and irreparable damage to the panels occurs on the ground and fourth storey. Concerning the structural members, 22%, 72%, and 81% of columns, and 18%, 68%, and 76% of beams are in unsafe conditions at the SDE, BDE, and MCE, respectively. The demand/capacity ratios for the unsafe columns at the BDE are greater than 2 on all storeys, reaching maximum values of 2.68.

– The ADAS-based retrofit solution allows to limit the panel drift ratios below 0.65%, denoting easily repairable damage conditions, on the first and second storey, and below the IO-related 0.5% limit on the remaining storeys. At the MCE the drift ratios are well below the technical repairability threshold for all storeys except the first, where the lower limit of this range is only slightly exceeded ($D_{pr,max}$ = 0.81%). The drift reductions achieved at the SDE are entirely caused by the stiffening effects of the protection system, while at the BDE and the MCE the dissipative action of the ADAS devices is activated. The demand/capacity ratios of

the structural members do not exceed 1.25 on the ground storey and 1.05 on the first storey, for columns, and 1.18 for beams on the ground storey; local strengthening interventions with single sheets of CFR fabrics are sufficient to bring these members to safe conditions. The flanges of the foundation beams parallel to *X* must be widened to safely absorb the increase in the stress states on the soil induced by the bracing effect of the protection system.

– The reduction factors on the peak panel drift ratios produced by the PFV-based intervention are approximately 15% higher than those obtained by the ADAS-based one. The infill drift profiles are also more homogeneous and smoothed along the building height. All columns and beams, as well as the foundations, are in safe conditions, not requiring additional strengthening measures.

– Increasing the numbers of ADAS damper plates, and incorporating more C-type PFV spring-dampers instead of B-type, or B-type instead of A-type ones, would not produce appreciable benefits. Therefore, the two design interventions, and the related estimated costs, represent almost "optimized" solutions from a technical viewpoint. The 4% higher amount of cost estimated for the PFV-based retrofit design is compensated by the fact that, unlike ADAS dampers, they would not need to be replaced after a seismic event of severity comparable to the BDE, or even the MCE.

– The dissipative bracing systems are positioned in the same eight vertical alignments along *Y*, where they are hidden by infills, and four alignments in *X*, located in the lateral spans of the two main façades. The remaining four alignments of the system equipped with the ADAS devices are situated on the two central portions of the main façades, whereas the remaining two of the system incorporating the PFV spring-dampers are hidden in an internal and an external infill. This determines a lower architectural impact of the PFV-based retrofit solution

ACKNOWLEDGMENTS

The study reported in this paper was sponsored by the Italian Department of Civil Protection within the ReLUIS-DPC Project 2024/2026, WP 15 "Devices and systems for base isolation and supplemental damping dissipation". The authors gratefully acknowledge this financial support.

REFERENCES

[1] A. Masi, L. Chiauzzi, G. Santarsiero et al., Seismic response of RC buildings during the Mw 6.0 August 24, 2016 Central Italy earthquake: the Amatrice case study. *Bulletin of Earthquake Engineering,* **17**, 5631-5654, 2019.

[2] G. Terenzi, I. Costoli, S. Sorace, Activation control extension of a design method of fluid viscous dissipative bracing systems. *Bulletin of Earthquake Engineering,* **18(8)**, 4017-4038, 2020.

[3] D. De Domenico, G. Ricciardi, I. Takewaki, Design strategies of viscous dampers for seismic protection of building structures: a review. *Soil Dynamics and Earthquake Engineering*, **118**, 144-165, 2019.

[4] S. Sorace, G. Terenzi, Seismic protection of frame structures by fluid viscous damped braces. *ASCE Journal of Structural Engineering,* **134(1)**, 45-55, 2008.

[5] Ministerial Decree 24 January 1986. *Norme tecniche relative alle costruzioni sismiche*. Italian Ministry of Public Works, Rome, Italy, GU no. 08 – 1986 (in Italian).

[6] G. Terenzi, Novel design procedure for steel hysteretic dampers in seismic retrofit of frame structures. *Engineering Structures*, **284**, Paper no. 115969, 2023.

[7] CSI, SAP2000NL. *Theoretical and user's manual*. Release 25.09. Computers & Structures Inc., Berkeley, CA, USA, 2024.

[8] B. Stafford Smith, Behaviour of square infilled frames. *ASCE Journal of the Structural Division*, **92(1),** 381-403, 1966.

[9] S.H. Bertholdi, L.D. Decanini, C. Gavarini, Telai tamponati soggetti ad azione sismica, un modello semplificato: confronto sperimentale e numerico. *Proceedings of the VI Italian National Conference on Earthquake Engineering*, University of Perugia Press, Perugia, Italy, 2, 815-824, 1993 (in Italian).

[10] S. Sorace, I. Costoli, G. Terenzi, Seismic assessment and dissipative bracing retrofit-based protection of infills and partitions in RC structures. *Engineering Structures,* **281**, Paper no.115781, 2023.

[11] G. Mucedero, D. Perrone, E. Brunesi, R. Monteiro, Numerical modelling and validation of the response of masonry infilled RC frames using experimental testing results. *Buildings*, 10(10), **182**, 2021.

[12] M. Gaetani d'Aragona, M. Polese, A. Prota, Effect of masonry infill constitutive law on the global response of infilled RC buildings. *Buildings*, 11(2), **57**, 2021.

[13] IMIT, *Update of Technical Standards for constructions*. Italian Ministry of Infrastructure and Transport, Rome, Italy, Ministerial Decree 17 January 2018 – GU no. 42-2018 (in Italian).

[14] S. Sorace, G. Terenzi, C. Mori, Passive energy dissipation-based retrofit strategies for R/C frame water towers. *Engineering Structures,* **106**, 385-398, 2016.

[15] E. Gandelli, D. De Domenico, V. Quaglini, Cyclic engagement of hysteretic steel dampers in braced buildings: a parametric investigation. *Bulletin of Earthquake Engineering,* **19**, 5219-5251, 2021.

[16] E. Martinez-Romero, Experiences on the use of supplemental energy dissipators on building structures. *Earthquake Spectra*, **9(3)**, 581-624, 1993.

[17] S. Sorace, G. Terenzi, Non-linear dynamic modelling and design procedure of FV spring-dampers for base isolation. *Engineering Structures*, **23**, 1556-1567, 2001.

[18] G. Terenzi, Energy-based design criterion of dissipative bracing systems for seismic retrofit of framed structures. *Applied Sciences*, **8(2),** 0268, 2018.

[19] Dyna Shock System, URL http://www.dynashocksystem.com/ [accessed 13 November 2024].